Performance and mechanisms of heterotrophic nitrification aerobic denitrifying bacteria in utilizing photogenerated electrons from magnetite for efficient denitrification

Liu, G.; Liu, D.; Hu, M.; Ren, X.; Ran, Y.; Luo, T.; Peijnenburg, W.J.G.M.

Journal of Water Process Engineering 70 (2025) 106942

Contents lists available at ScienceDirect

Journal of Water Process Engineering

journal homepage: www.elsevier.com/locate/jwpe

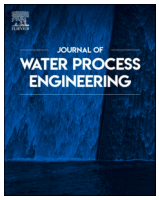

Performance and mechanisms of heterotrophic nitrification aerobic denitrifying bacteria in utilizing photogenerated electrons from magnetite for efficient denitrification

Guo Liu [a,b,c], Dian Liu [a,b,c], Mengyao Hu [a,b,c], Xi Ren [a,b,c], Yueyu Ran [a,b,c], Tianlie Luo [a,b,c,*], Willie J.G.M. Peijnenburg [d,e]

[a] State Key Laboratory of Geohazard Prevention and Geoenvironment Protection, Chengdu University of Technology, Chengdu 610059, China
[b] State Environmental Protection Key Laboratory of Synergetic Control and Joint Remediation for Soil & Water Pollution, Chengdu University of Technology, Chengdu 610059, China
[c] College of Ecology and Environment, Chengdu University of Technology, Chengdu 610059, China
[d] Institute of Environmental Sciences (CML), Leiden University, Leiden 2300, RA, the Netherlands
[e] National Institute of Public Health and the Environment, Centre for the Safety of Substances and Products, Bilthoven 3720, BA, the Netherlands

ARTICLE INFO

Editor: Rong Chen

Keywords:
Magnetite
HN-AD bacteria
Photogenerated electrons
Denitrification mechanism
Sunlight irradiation

ABSTRACT

Heterotrophic nitrification-aerobic denitrification bacteria (HN-AD) have been demonstrated to possess denitrification potential. The limited effectiveness of HN-AD in remediating nitrogen-polluted surface waters is attributed to its low C/N ratio. In this study, a magnetite photogenerated electrons coupled HN-AD bacteria system was constructed and its nitrogen removal mechanisms were revealed. The results demonstrated the electrons photo-generated by magnetite can effectively stimulate the growth of the HN-AD *(Delftia sp.,* Y19).The coupled system of the ammonium and nitrate reached removal rates of 80.1 % and 71.3 %, which were 4 times higher than the strain Y19 alone (20.3 %, 15.2 %). Compared with dark conditions, the activity of enzymes (AMO, HAO, NAR and NIR) related to nitrogen removal in Y19 was increased by 4.81, 4.75, 6.45 and 4.78 times under sunlight irradiation, respectively. This suggests that the electrons photo-generated from magnetite can enhance the metabolic activities of the Y19 strain. Furthermore, the concentration of ferric ions dissolved from magnetite has been detected as equaling 0.13 mg/L, which plays a crucial role in the reduction of nitrate. The denitrification mechanisms of the coupled system can be incorporated: heterotrophic nitrification and aerobic denitrification by strain Y19, photogenerated electrons reduction of magnetite, the reduction of ferric ions, and the adsorption of magnetite. After 9 days of running the simulator, the magnetite-Y19 coupled system achieved removal rates of 100 % for nitrate and chemical oxygen demand, and 36 % for ammonium. This study offers novel insights into the utilization of photogenerated electrons by microorganisms for remediating the low C/N ratio wastewater.

1. Introduction

Nitrogen pollution primarily arises from the excessive utilization of nitrogenous fertilizers and the discharge of both industrial wastewater and domestic sewage [1,3].The inherent self-purification capacity of water bodies is insufficient to effectively eliminate the surplus of nitrogenous contaminants, resulting in their accumulation in wastewater and posing a threat to ecological and environmental health [2]. It

Abbreviations: Y19, *Delftia sp.,* Y19; HN-AD, heterotrophic nitrification-aerobic denitrification bacteria; AMO, ammonia monooxygenase; HAO, hydroxylamine oxidoreductase; NAR, nitrate reductase; NIR, nitrite reductase; EET, extracellular electron transfer; FTO, fluorine-doped tin oxide; LB, luria-bertani; PBS, phosphate buffered saline; OD_{600}, optical density at 600 nm; CV, cyclic voltammetry; LSV, linear sweep voltammetry; DNA, deoxyribonucleic acid; PCR, polymerase chain reaction; PE250, paired-end 250; COD, chemical oxygen demand; EPSs, extracellular polymeric substances; DPV, differential pulse voltammetry; OTU, operational taxonomic unit; SEM, scanning electron microscopy; NO_2^-, nitrite; NH_4^+-N, ammonium; NO_3^-, nitrate.

* Corresponding author at: State Key Laboratory of Geohazard Prevention and Geoenvironment Protection, Chengdu University of Technology, Chengdu 610059, China.

E-mail address: luotianlie19@cdut.edu.cn (T. Luo).

https://doi.org/10.1016/j.jwpe.2025.106942
Received 29 October 2024; Received in revised form 30 December 2024; Accepted 2 January 2025
Available online 15 January 2025

is therefore imperative to remediate nitrogenous contaminants from aqueous system.

Physicochemical and biological methods are the primary approaches employed for the removal of nitrogen-containing pollutants [4]. Nevertheless, physicochemical technologies exhibit several drawbacks including limited efficacy, high costs, restricted operational conditions, and potential secondary pollution. Biological nitrogen removal technology has gained widespread recognition as a cost-effective and environmentally friendly strategy for eliminating nitrogen [1,5,6]. In comparison to traditional biological denitrification technologies, heterotrophic nitrification - aerobic denitrification (HN-AD) bacteria can achieve the integration of both nitrification and denitrification processes [7]. The HN-AD bacteria contribute to the stability of the system pH value and enhance overall system stability. Furthermore, these bacteria exhibit rapid growth and metabolism, facilitating simultaneous degradation of chemical oxygen demand (COD) and ammonium (NH_4^+) while working in conjunction with aerobic denitrification to improve COD removal efficiency.

Recent studies have demonstrated that inoculating wastewater treatment facilities with HN-AD bacteria can enhance nitrogen removal by up to 50 % [8]. Therefore, HN-AD bacteria show promising potential for treating nitrogen pollution. However, this process requires sufficient extracellular organic carbon as an electron donor [9], which is crucial for ensuring optimal nitrogen removal performance of HN-AD bacteria. Additionally, the low carbon to nitrogen (C/N) ratio limits the effectiveness of HN-AD bacteria in remediating surface water bodies such as rivers and lakes [10]. Currently, it is necessary to explore additional organic carbon sources under oligotrophic conditions in order to study the denitrification capabilities of HN-AD bacteria without external carbon sources. Thus, identifying suitable electron donors becomes pivotal for advancing the development of HN-AD bacterial technology.

Due to the inherent advantages of biological denitrification, extensive research efforts have been dedicated towards enhancing its efficiency through environmentally compatible and non-polluting means. Exploring the utilization of extracellular electrons to augment microbial denitrification efficiency represents a promising avenue for further investigation. Notably, the introduction of nano-zero-valent iron has been found to enhance microorganism-mediated extracellular electron transfer (EET), resulting in accelerated nitrate and ammonia removal within low C/N ratio wastewater systems [11]. Additionally, graphene has demonstrated an ability to improve microbial EET processes and increase NO_3^- removal rates by 17 % even at low temperatures [12]. Therefore, whether involving the provision of additional extracellular electrons or facilitation of electronic dielectric conduction, these strategies possess the potential to enable microorganisms to efficiently carry out biological denitrification under conditions characterized by limited organic substrates or extreme circumstances [13].

Natural soils and sediments harbor a wide variety of semiconductor minerals, which can provide exogenous electrons for the growth and metabolism of microorganisms [14,15]. Among these, magnetite is abundant in nature and can facilitate microbial functions by generating electrons through photoexcitation or by enhancing extracellular electron transfer. The incorporation of magnetite can enhance the anaerobic microorganism-mediated degradation of benzoic acid and concurrently stimulate methane production by syntrophic microorganisms [16]. Moreover, magnetite possesses excellent conductive properties, enabling it to function as an effective “bridge” for the transmission of electronic signals between symbiotic bacteria. It is hypothesized that the widely existing magnetite in nature promotes the metabolism of denitrifying microorganisms by generating electrons, thereby enhancing their denitrification function.

In this study, the highly efficient denitrifying strain of HN-AD bacteria, *Delftia sp.* Y19, was isolated and characterized. Subsequently, the utilization of magnetite photogenerated electrons by strain Y19 and its photoelectrochemical response were investigated through electrochemical analysis, leading to the construction of a magnetite-Y19 coupled system. Additionally, the denitrification efficacy of this integrated system was assessed by investigating the impacts of magnetite and microbial dosage on the removal efficiency of ammonia nitrogen and nitrate nitrogen as target contaminants. Changes in denitrification related enzyme activity including microbial ammonia monooxygenase (AMO), microbial hydroxylamine oxidoreductase (HAO), microbial nitrite reductase (NIR) and microbial nitrate reductase (NAR) among different systems were determined to gain insights into the underlying denitrification mechanism. Finally, simulating an actual water environment enabled the evaluation of nitrogen removal efficiency in low C/N ratio wastewater using the developed integrated system, while simultaneously analyzing patterns of pollutant elimination. The microbial community structure within the device was investigated using high-throughput sequencing, enabling assessment of both diversity and relative abundance of microbial populations. This research provides theoretical references and data support for harnessing semiconductor mineral photogenerated electrons by microorganisms in treating low C/N ratio wastewater.

2. Materials and methods

2.1. Chemicals

Magnetite was prepared from natural magnetite in Zhengzhou City, Henan Province, China. The magnet ore was washed several times with tap water, and then washed with deionized water. After removing the surface impurities, it was dried in a 60 °C oven and ground to 200 mesh, sealed and stored. Other chemical reagents, including glucose, potassium dihydrogen phosphate, dipotassium phosphate, were purchased from the Chengdu Kelong Chemical Reagent Factory in Chengdu City, Sichuan Province, China.

2.2. Screening and culturing of strains

The heterotrophic nitrification-aerobic denitrification bacteria (HN-AD) were screened from the Yuexi River in Anyue County, Ziyang City, Sichuan Province, China. The medium type and formula used in the screening process are provided in the supporting information (Table S1). HN-AD bacteria with denitrification ability (strain Y19) were obtained after enrichment, preliminary screening, re-screening and domestication [5,17]. The screening process of HN-AD and phylogenetic tree of Y19 is described and visualized in Text S1 and Fig. S1, respectively.

2.3. Ability of HN-AD bacteria to utilize the photogenerated electrons of magnetite

2.3.1. Electrochemical testing

Thirty milligram of magnetite was grinded to 200 mesh sieve and mixed with 100 μL of 5 % nafion reagent. The mixture was smeared on a 20 mm × 20 mm × 1.1 mm FTO electrode with a glass rod. The fluorine-doped tin oxide (FTO) electrode was ultrasonically cleaned twice with anhydrous ethanol and deionized water to remove surface impurities and dried at 60 °C for later use. The conductive surface was measured with a multimeter, and the magnetite was evenly applied to the conductive surface. The magnetite-coated FTO electrode served as the working electrode, the Ag/AgCl electrode was used as the reference electrode, and the platinum wire electrode was the counter electrode. The electrolyte was an luria-bertani (LB) medium solution with 0.1 mol/L KH_2PO_4 added. Take 5 mL of the bacterial suspension diluted with phosphate buffered saline (PBS), add it to 100 mL of the culture medium solution. The test begins after 2 h of reaction in the dark. Experimental schematic diagram is visualized Fig. S2.

2.3.2. Measurement of the growth curve

Collect 5 mL of the bacterial suspension that has been cultured to the logarithmic phase (after 12 h) into a centrifuge tube, and centrifuge at

8000 rpm for 5 min. The bacterial suspension was diluted with PBS buffer to optical density at 600 nm (OD_{600}) at 0.5. Then, it was added to a quartz single-chamber reactor containing 100 mL denitrification medium, placed in a constant temperature shaker at 30 °C and 120 r/min, irradiated with a 300 W xenon lamp (DY300G, Guangzhou Xingchuang Electronics Co., Ltd., China) and cultured for 96 h. Due to its relatively high light power density and spectrum, 300 W xenon lamp is often adopted as a light source for simulating sunlight irradiation. Furthermore, direct exposure to outdoor sunlight introduces additional influencing factors, including humidity and temperature, which may lead to inconsistencies and a lack of reproducibility in experimental results [18–20]. The growth curve was recorded. The control group was a device wrapped with tin foil paper under the same conditions. The experimental schematic diagram is visualized in Fig. S3.

2.4. Performance and denitrification mechanism

2.4.1. Influences of the dosage of magnetite and the dosage of the strain

The effects of the magnetite (g/L) and the Y19 dosage (*v*/v) on nitrogen removal of the magnetite-Y19 coupled system were investigated using single factor experiments. Based on the magnetite dosage range in wastewater, three levels of magnetite dosage (1, 2 and 5 g/L) were designed to investigate their effect on nitrogen removal in the coupled system, as well as using a Y19 dosage of 1 %, respectively. Dosages of magnetite (g/L) and the Y19 (*v*/v) on nitrogen removal in the coupled system are shown in Table S2. The experimental wastewater volume of each experimental group was 300 mL and the dosage of the trace elements was 1 mL/L. Then, the pH value of the reactors was adjusted to 7. The experimental schematic diagram is visualized in Fig. S4.

2.4.2. Denitrification performance of the coupled system

To verify the ability of strain Y19 to utilize magnetite, samples comprising magnetite-Y19 (light), Y19 (light), and magnetite-Y19 (dark) were prepared. Y19 (dark) was not set because light will affect the removal of nitrate and COD in the system. The concentrations of nitrate (NO_3^--N), NH_4^+-N and COD in the simulated wastewater were set at 20 mg/L, 20 mg/L and 40 mg/L, respectively. Each experimental group was placed in a 120 r/min device and the irradiation of the reactor was performed using a 300 W xenon lamp. All experiments were performed at 30 °C and each experiment had three replicates. Samples were collected every 24 h during the experiment and the obtained samples were filtered through a 0.45 μm filter membrane. Finally, the changes of pH value in each group were recorded. The experimental schematic diagram is visualized in Fig. S5.

2.4.3. Enzymes assay

The activities of denitrification enzymes in different systems were determined during denitrification. Water samples of the above three systems were taken at different time periods. Enzyme activity was determined by enzyme assay kits. The enzyme kit was adopted comprising microbial ammonia monooxygenase (AMO) ELISA kit, microbial hydroxylamine oxidoreductase (HAO) ELISA kit, microbial nitrite reductase (NIR) ELISA kit, and microbial nitrate reductase (NAR) ELISA kit. The specific operation was carried out according to the manufacturer's instructions (Shanghai Enzyme-Linked Biotechnology Co., Ltd., China).

2.4.4. Redox analysis

To study the redox characteristics of the magnetite-Y19 system in simulated wastewater under simulated sunlight, the cyclic voltammetry (CV) curve, differential pulse voltammetry (DPV) and the linear sweep voltammetry (LSV) curve were measured by means of an electrochemical workstation. Take 3 mL of the bacterial suspension diluted with PBS in Section 2.3 and add it to 100 mL of the simulated wastewater. The device is placed on an oscillator at 120 r/min for a reaction lasting 72 h.

2.5. Application of magnetite-Y19 coupled system

2.5.1. Denitrification performance

To investigate the remediation performance of the coupled system in actual wastewater, we designed an experimental device with a material of organic glass cylinder, a height of 35 cm and a diameter of 5 cm (Fig. S6). To enable more microorganisms in the device, a 0.1 m thick layer of sediment from Yuxi River in Anyue County, Ziyang City, China, was placed at the bottom of the device. The volume of the wastewater is 350 mL. Two experimental groups, namely the Y19 system group and the coupled system group, were established to investigate the denitrification performance of the coupled system. One gram of magnetite was added to the coupled system group and 10 mL strain Y19 were added to both two groups. All of the experiments were conducted with indoor illumination at temperatures ranging from 15 to 25 °C. The experiments lasted 9 days, and samples were collected at 11 a.m. every day. The water samples were filtered using a 0.45 μm filter to determine the concentrations of NH_4^+-N, NO_3^--N, NO_2^--N (nitrite), COD and pH value. The experimental wastewater was prepared using substances such as NH_4Cl, KNO_3, and $C_6H_{12}O_6$. The wastewater primarily contains 20 mg/L NH_4^+-N, 20 mg/L NO_3^--N and 400 mg/L COD.

2.5.2. Microbial metagenomic sequencing analysis

Metagenomic microbial taxonomic high-throughput sequencing and analyses were performed on the microbial community structure before and after the reaction. Firstly, the bacterial liquid sample was pretreated to extract genomic deoxyribonucleic acid (DNA) in the sample, and the DNA integrity of the extracted sample was detected by agarose gel electrophoresis. The primers used were 515F (5'-GTGYCAGCMGCCGCGGTAA-3′) and 806R (5'-GGACTACNNGGGTATCTAAT-3′) for polymerase chain reaction (PCR) amplification. Target fragments were detected by 2 % agarose gel electrophoresis. And the paired-end 250 (PE250) sequencing method was used. The sequencing reagents were provided by Illumina, using the Hiseq Rapid SBS Kit v2 (FC-402-4023 500 Cycle). All samples were treated and sent to Chengdu Luoning Biotechnology Technology Company in Chengdu City, Sichuan Province, China, for high-throughput sequencing. The initial Y19 group of water samples was designated as D0, the Y19 group after the reaction was labeled as Y19, and the magnetite-Y19 group was identified as DYM.

2.6. Analytical method

The concentrations of NO_3^--N, NO_2^--N, NH_4^+-N and COD were measured according to the standard methods for the examination of water and wastewater (Table S3).

3. Results and discussion

3.1. HN-AD utilizes photogenerated electrons for growth

To illustrate the capability of strain Y19 to grow by utilizing photogenerated electrons from magnetite, a series of control experiments were designed. The Y19 (light) condition was omitted due to the presence of ultraviolet bands in the simulated sunlight, which could inhibit the growth of strain Y19. As shown in Fig. 1a, the maximum OD_{600} as observed in magnetite-Y19(light) was 0.237, which was higher than the OD_{600} in the other controls after 72 h of cultivation. This finding indicates that the photogenerated electrons generated by magnetite under light excitation can effectively stimulate and promote the growth of strain Y19 [21].

After 72 h of cultivation, the OD_{600} of strain Y19 decreased. This can be attributed to the attachment of microorganisms to the surface of magnetite, which affects the conversion of light energy by the magnetite. The covering of minerals by microbial species leads to a reduction in the generation of photogenerated electrons. And the nutrients in the culture medium have been exhausted, restricting the growth of

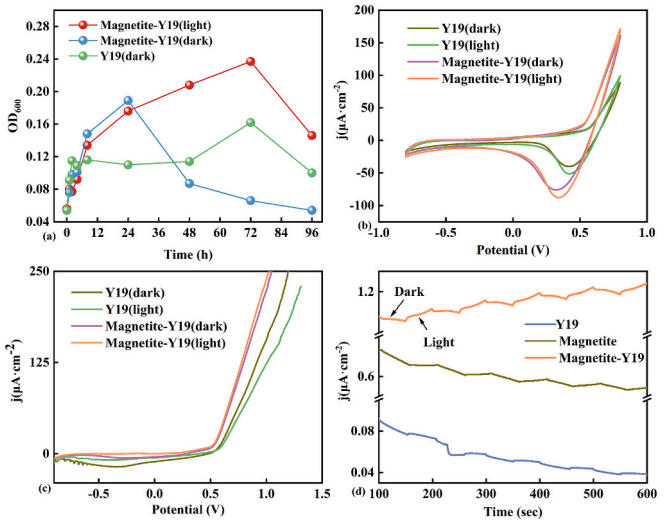

Fig. 1. (a) Growth curve of strain Y19 under light. (b) Cyclic voltammetry curve. (c) Linear sweep voltammetry curve. (d) Change curve of current with time.

microorganisms. Furthermore, the adhesion of strain Y19 results in a lower concentration of microorganisms in the suspension. In comparison to the end of the experiment, the distribution of magnetite was relatively dispersed prior to the experiment (Fig. S7). The strain Y19 may form a biofilm on the surface of magnetite, suggesting that magnetite could provide attachment sites for the strain Y19 [22].

Subsequently, the FTO electrode coated with magnetite was employed as the working electrode to investigate the electrochemical activity between magnetite and strain Y19. In comparison to other systems, the current intensity of the magnetite-Y19 (light) system exhibits a significant increase. This indicates that under the influence of light, the extracellular electron transfer capabilities of microorganisms are enhanced, allowing for rapid electron transfer to the magnetite electrode. Furthermore, light itself cannot significantly induce a shift in the reduction peak (Fig. 1b). Thus, the direct influence of simulated sunlight on magnetite can be excluded.

Before 0.5 V, all systems exhibited a lower current intensity due to the rapid recombination of photogenerated electrons and holes (Fig. 1c) [23]. However, after 0.5 V, the magnetite-Y19 system demonstrated a significant increase in photocurrent intensity, reaching a maximum value of 250 $\mu A \cdot cm^{-2}$ (Fig. S8). These results indicate that the extracellular electrons generated by strain Y19, along with the photogenerated charges produced by magnetite, are effectively driven by the external circuit. This facilitates the rapid separation and transfer of photogenerated electrons [24,25]. In addition, both strain Y19 and magnetite exhibit photo-responsive properties (Fig. 1d). However, the photocurrent intensity of the coupled system increases significantly, suggesting that the coupled system generates a greater number of charges under illumination, allowing for the effective separation of e^- and holes h^+ [26].

3.2. *Effects of the key parameters of magnetite-Y19 coupled system*

Generally, the removal rates of NO_3^--N, NH_4^+-N and COD exhibited a gradual upward trend (Fig. 2). The removal rates of NO_3^--N, NH_4^+-N and COD did not increase proportionally with the increasing dosage of magnetite. However, the concentration of NO_2^--N exhibited an upward trend (Fig. 2c) with varying degrees of NO_2^--N accumulation observed across each gradient. This phenomenon may be associated with the denitrification pathway of strain Y19. When the dosage of magnetite was 5 g/L, the concentration of NO_2^--N reached 8.7 mg/L. This indicates that the dosage of magnetite was excessive, leading to its agglomeration and to a decrease in both e^- and h^+ [27].

The removal rates of NO_3^--N, NH_4^+-N and COD exhibited an increasing trend upon increasing dosage of strain Y19 (Fig. 3). When the dosage of strain Y19 reached 7 %, the removal rate of NO_3^--N peaked at 24 h. Concurrently, COD was rapidly eliminated, leading to a depletion

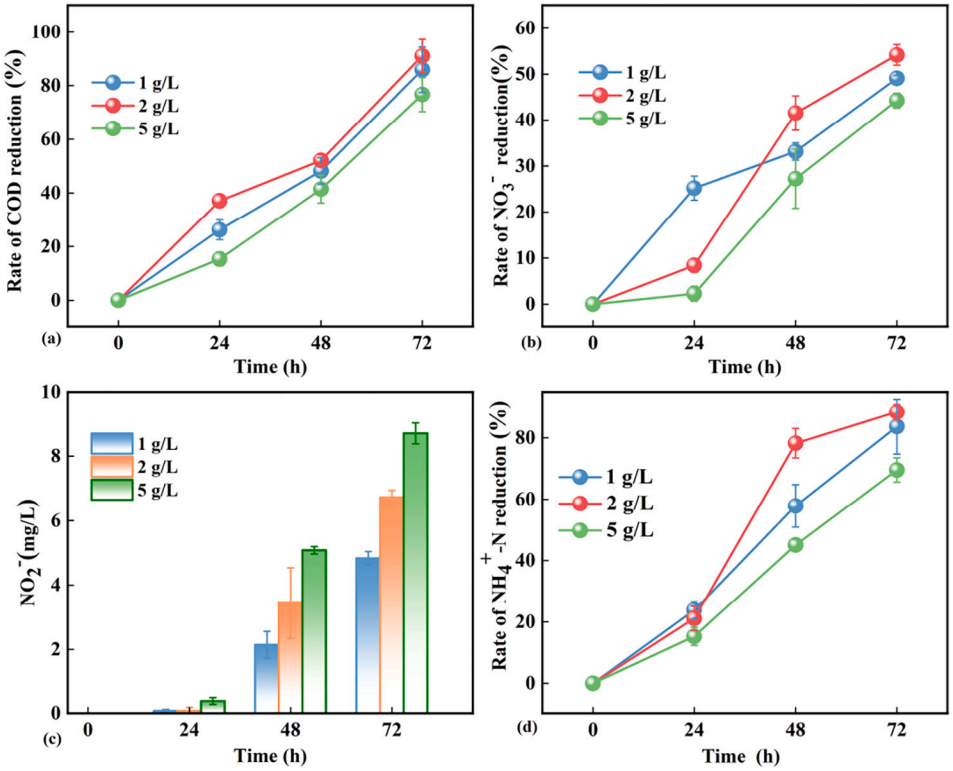

Fig. 2. Nitrogen removal capacity of the system under different magnetite dosage conditions.

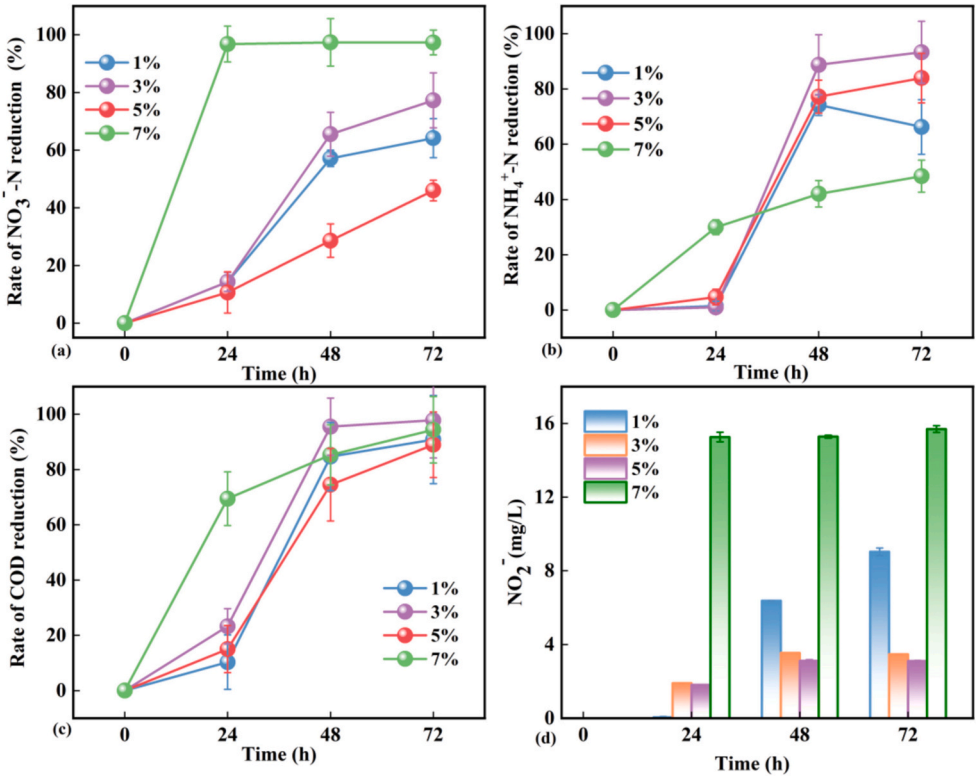

Fig. 3. Denitrification capacity of the system under different strain dosage conditions.

of organic carbon sources in strain Y19. Due to the excessive addition of strain Y19, a biofilm rapidly formed on the surface of magnetite. This phenomenon leads to a reduction in electron production by magnetite and an incomplete conversion of nitrogen. When the dosage of strain Y19 was 3 %, the removal rates for NO_3^--N, NH_4^+-N and COD were observed to be 77.3 %, 93.2 % and 96 %, respectively. The accumulation of NO_2^--N reached a concentration of 3.4 mg/L. As the dosage of strain Y19 was further increased, no further enhancement in removal rates was noted. Therefore, a dosage of 3 % for strain Y19 is deemed the most effective for promoting denitrification within the coupled system.

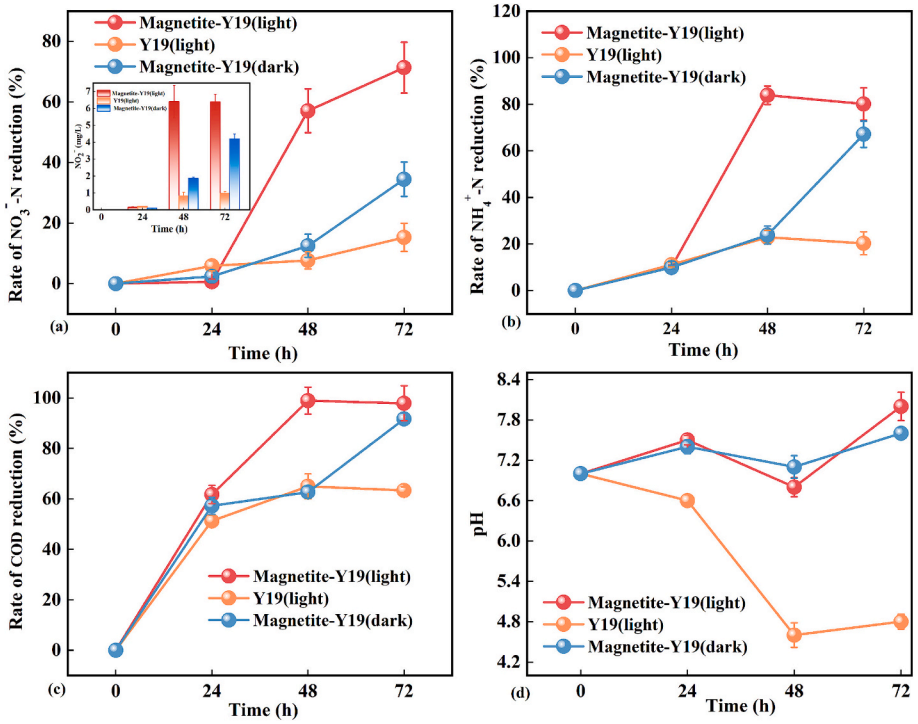

Fig. 4. Denitrification performance of different systems.

3.3. Denitrification performance of magnetite-Y19 coupled system

The denitrification capacity of the magnetite-Y19 (light) system was significantly superior to that of the other systems (Fig. 4). The removal rates of NH_4^+-N, NO_3^--N and COD by the magnetite-Y19 (light) system were 71.3 %, 80.1 % and 97.9 %, respectively. These results demonstrate that in the case of insufficient organic carbon sources, strain Y19 can utilize the photogenerated electrons generated by magnetite to carry out growth metabolic activities and denitrification. The removal rate of NH_4^+-N was found to be increasing up to 48 h (Fig. 4b), suggesting that there is no microbial death resulting in the release of intracellular nitrogen during this process [28]. Under illumination, h^+ was produced extracellularly. In contrast to the single microbial system, the ferric ions (Fe^{2+}) and Fe^{3+} cycles within the magnetite of the coupled system can utilize the generated h^+. This interaction helps maintain a weakly alkaline pH value in the system, which is advantageous for denitrification processes.

The removal rates of NO_3^--N and NH_4^+-N plateaued after 72 h, while the concentration of NO_2^--N reached approximately 6 mg/L. This suggests that NO_3^--N was not completely eliminated. When the organic carbon source is lacking, nitrite reductase is at a disadvantage in competing for electron acceptors and its enzymatic activity is inhibited (Fig. S10), while nitrate reductase remains active. The rate of nitrate reduction to nitrite is greater than that of nitrite reduction to nitrogen gas, resulting in the accumulation of NO_2^- [29,30]. When the reduction of NO_3^--N is greater, there tends to be a relatively higher accumulation of NO_2^--N [31].

3.4. Changes in microbial enzyme activity

Microorganisms, when confronted with external environmental stimuli, maintain the redox balance between their intracellular and extracellular environments by modulating the expression patterns of cytochromes, secreting extracellular polymeric substances (EPSs), and employing enzymatic metabolic processes [32]. The activities of the enzymes AMO, HAO, NAR, and NIR were found to be elevated in the coupled system (Fig. S10). Compared with dark conditions, the activity of enzymes (AMO, HAO, NAR and NIR) related to nitrogen removal in Y19 was increased by 4.81, 4.75, 6.45 and 4.78 times under sunlight irradiation, respectively. The findings indicated that in conditions where the organic carbon source was insufficient, the photogenerated electrons from magnetite positively influenced the metabolic activity of microorganisms.

NAR and NIR are two key enzymes that play crucial roles in the denitrification process. NAR is responsible for catalyzing the conversion of NO_3^--N to NO_2^--N, while NIR facilitates the transformation of NO_2^--N into nitrogen-containing gases. In the coupled system, the expression levels of both enzyme activities are notably elevated. This aligns with the nitrogen transformation observed during the previously mentioned denitrification process. Due to the necessity for NIR to reside in an anaerobic environment, the relatively high expression of NIR does not translate into the effective conversion of NO_2^--N to N_2 for removal. This inefficiency is exacerbated by the persistent aerobic conditions, leading to accumulation of NO_2^--N.

Microelement iron is one of the important elements for microbial growth and can promote extracellular electron transfer in microorganisms [33]. Based on the results of nitrogen removal and changes in enzyme activity, it was found that the coupled system also had a certain degree of nitrogen removal under dark conditions, so the changes in Fe (II) concentration in the coupled system under light and dark conditions were explored (Fig. S11a). The pH value of the coupled system will initially decrease (Fig. S9), promoting the dissolution of magnetite and resulting in an increase in the concentration of Fe(II) ions [34]. Under light conditions, the concentration of Fe(II) generated in the system was 0.13 mg/L, which may have been oxidized by the hydrogen ions produced by magnetite. In the dark system, the concentration of Fe(II) was 0.44 mg/L at the end of the experiment. The removal rates of NO_3^--N and NH_4^+-N by the coupled system were 34.5 % and 67.1 %, respectively. Meanwhile, Fe(II) participates in the enzyme synthesis process of denitrifying microorganisms, which can upregulate the expression of denitrification genes [35]. Therefore, in the dark conditions, all enzymes related to denitrification in the system showed certain activity.

3.5. Oxidation-reduction analysis

When the electrolyte was a simulated wastewater containing NO_3^--N and NH_4^+-N, significant oxidation-reduction peaks were observed at 0.51 V and − 0.22 V, indicating that oxidation and reduction reactions occurred in the coupled system. Magnetite-induced photocatalytic e-reduction of NO_3^--N occurs, while microorganisms utilize organic matter-derived organic acids to consume h^+. The portion of Fe^{2+} that is dissolved from magnetite can be oxidized to Fe^{3+} by NO_3^-, and strain Y19 converts NO_3^--N and NH_4^+-N through oxidation-reduction reactions.

The DPV curve shows a distinct peak intensity, and it varies significantly at different potentials (Fig. S11c). The photocatalytically generated electrons can be transferred and separated effectively. After 0.7 V, the system showed a higher light current intensity, indicating that the photogenerated electrons generated by the system and the extracellular electrons produced by the microorganisms had rapidly passed to the surface of the magnetic iron oxide electrode (Fig. S11d). The strain Y19 was able to transfer extracellular electrons between the magnetic iron oxide electrode and itself, indicating strong catalytic oxidation-reduction reactions.

3.6. Mechanism and denitrification pathways

After conducting a thorough analysis, we propose a potential mechanism by which the coupled system influences nitrate reduction. This mechanism is illustrated in Fig. 5. The mechanism primarily encompasses four key aspects: the heterotrophic nitrification and aerobic denitrification of Y19, the photogenerated electrons reduction of magnetite, the reduction of Fe (II) and the adsorption of magnetite.

Magnetite can generate e^- and h^+ under light conditions, allowing for their effective separation. The generated electrons are capable of reducing NO_3^- to NO_2^-, NH_4^+ and N_2 with NO_3^- serving as the substrate. The organic acid generated through nitrification can be oxidized by h^+ to facilitate the removal of e^- (Eq. (7)). The dissolved portion of Fe^{2+} from magnetite was 0.13 mg/L which was involved in the reduction of nitrate ions. (Eq. (8)) [36]. In the coupled system, magnetite can function as an electron mediator or acceptor for microorganisms. Additionally, it may adsorb anions such as NO_3^- and NO_2^- prior to electron transfer, forming complexes at the surface of magnetite. This interaction can lead to a reduction in the concentration of NO_3^- in aqueous solutions [37].

$$NH_4^+ + 2\,O_2 \rightarrow NO_3^- + 2H^+ + 2H_2O \quad (1)$$

$$NO_3^- + 2\,e^- + 2H^+ \rightarrow NO_2^- + H_2O \quad (2)$$

$$NO_3^- + 8\,e^- + 10H^+ \rightarrow NH_4^+ + 3\,H_2O \quad (3)$$

$$2\,NO_3^- + 10\,e^- + 12H^+ \rightarrow N_2 + 6\,H_2O \quad (4)$$

$$NO_2^- + 6\,e^- + 8H^+ \rightarrow NH_4^+ + 2\,H_2O \quad (5)$$

$$2\,NO_2^- + 6\,e^- + 8H^+ \rightarrow N_2 + 4\,H_2O \quad (6)$$

$$HCOO^- + h^+ \rightarrow H^+ + \cdot CO_2^- \quad (7)$$

$$Fe^{2+} + 2\,NO_3^- + 24\,H_2O \rightarrow 10\,Fe(OH)_3 + N_2 + 18H^+ \quad (8)$$

HN-AD bacteria played a crucial role in the removal of NH_4^+ and NO_3^- in the coupled system. The majority of NH_4^+, NO_3^-, and COD were

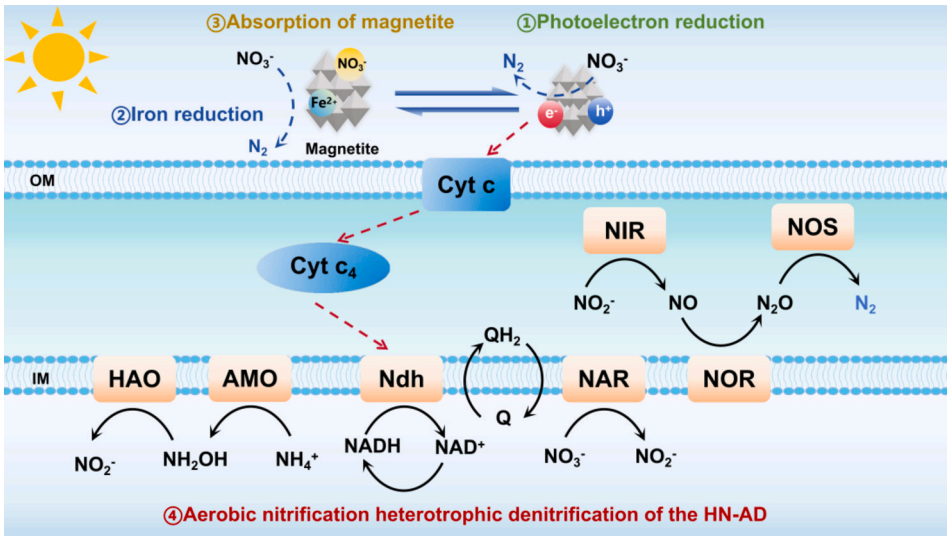

Fig. 5. Denitrification mechanism of magnetite-Y19 system under simulated sunlight irradiation.

effectively eliminated by microbial activity. The metabolic pathways of ammonia nitrogen in HN-AD are currently believed to involve two predominant mechanisms [34]: (1) $NH_4^+ \rightarrow NH_2OH \rightarrow NO_2^- \rightarrow NO_3^-$; (2) $NH_4^+ \rightarrow NH_2OH \rightarrow NO$. However, there was NO_2^- accumulation in the system. Therefore, the metabolic pathway of HN-AD bacteria is most likely $NH_4^+ \rightarrow NH_2OH \rightarrow NO_2^- \rightarrow NO_3^-$, and the aerobic denitrification pathway is $NO_3^- \rightarrow NO_2^- \rightarrow NO \rightarrow N_2O \rightarrow N_2$ (Fig. 5). The substrates examined in this study are NH_4^+ and NO_3^-. The presence of mixed pollutants exerts a selective effect on the substrate removal process carried out by strain Y19 [38], which leads to the accumulation of NO_2^-.

3.7. Application in actual wastewater

3.7.1. Denitrification performance

The experimental simulation device operates as a closed system without the continuous addition of a carbon source. After 9 days of operation, the COD and nitrate degradation rates within the system achieved 100 %. As illustrated in Fig. S9, the pH value levels of both systems initially decreased before subsequently increasing. Nevertheless, the coupled system exhibits more stable pH value levels. In the first four days, the strain Y19 system achieved a NO_3^--N removal rate of 87.9 %, while the removal rate of the magnetite-Y19 system was 80.8 % (Fig. 6a). These results indicate that strain Y19 exhibits a strong adaptability to its environment and can effectively mobilize indigenous microorganisms to facilitate denitrification. Compared to the magnetite-Y19 system, the concentration of NH_4^+-N in the strain Y19 system showed an increasing trend (Fig. 6b). This may be due to the release of ammonia nitrogen from the sediment, which is inhibited by magnetite. Additionally, there may be bacteria in the sediment that reduce nitrate to ammonia [39], and Liu et al. found that magnetite can inhibits the reduction function of this bacterium [34].

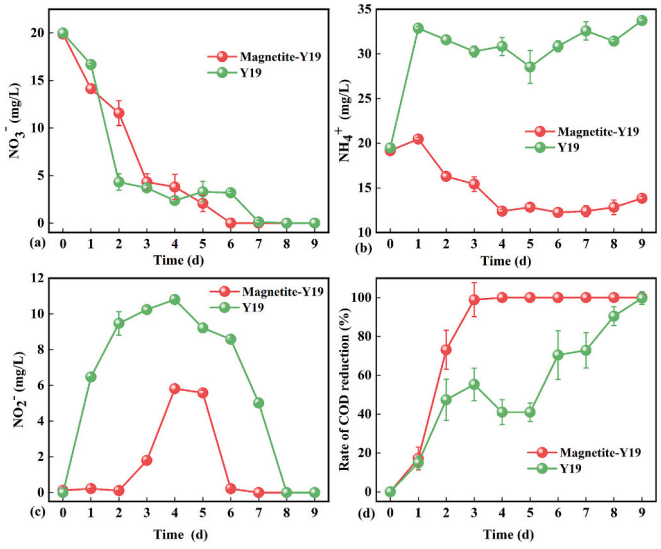

Fig. 6. Change of three nitrogen concentration and COD removal rate with time in the system.

The accumulation of NO_2^--N in the strain Y19 system peaked on the 5th day, reaching approximately 10.8 mg/L (Fig. 6c). As the reaction progressed, the denitrifying bacteria within the system gradually became dominant and initiated denitrification using NO_2^--N as the primary substrate. Ultimately, NO_2^--N was completely eliminated. The accumulation trend of NO_2^--N in the magnetite-Y19 system was similar to the trend in the Y19 system. However, the maximum accumulation was lower than that recorded in the Y19 system. This discrepancy may be attributed to a portion of the photogenerated electrons produced by magnetite being utilized for the reduction of NO_2^--N. The COD in the magnetite-Y19 system can be effectively reduced within approximately three days (Fig. 6d). It is plausible that the photogenerated electrons produced by magnetite facilitate interspecies electron transfer among various microorganisms present [40].

3.7.2. Analysis of microbial community structure succession

To investigate the impact of simulated light on the evolution of the microbial community structure in aquatic environments, water samples were collected for high-throughput sequencing. The richness and diversity of bacterial communities in these water samples, collected at various time points, are detailed in Table S4. At the end of the experiment there was a significant decrease in community richness. According to the Shannon and Simpson indices of species richness, the Shannon index for DYM was lower (high richness), while the Simpson index was higher. These findings indicate that the species richness in the magnetite-Y19 system is greater than that in the strain Y19 system. Therefore, under illumination, both the introduction of microorganisms and the addition of magnetite to the existing system will alter species richness and diversity. However, when magnetite is present, species richness tends to be relatively higher. It is evident that the most abundant operational taxonomic unit (OTU) across the three samples is Proteobacteria (Fig. 7a). Proteobacteria are Gram-negative bacteria that

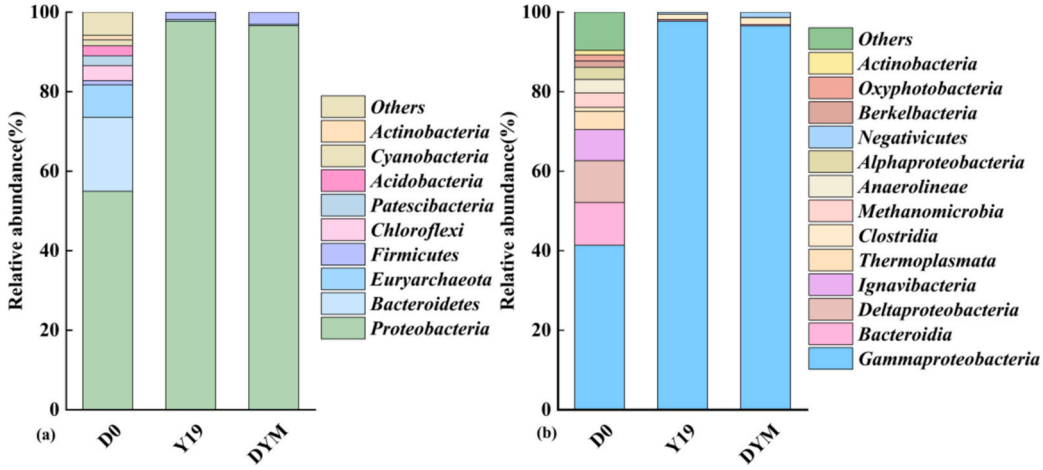

Fig. 7. Distribution of microorganisms at phylum (a) and class (b) levels.

play a significant role in the nitrogen transformation pathways involved in nitrification and denitrification processes [41–43]. In addition, all three samples contain Firmicutes. These bacteria play a crucial role in the denitrification process and possess the capability to degrade COD [44,45].

The microbial community in D0 exhibited a higher abundance compared to other samples, with Gammaproteobacteria γ identified as the predominant component. In both Y19 and DYM, Gammaproteobacteria γ was the dominant class, followed by Clostridia. Notably, Clostridia possess the capability to degrade COD [46]. There was minimal variation in the distribution of biological levels between the single strain and the coupled system, and the species structure remained relatively simple (Fig. 8a). A significant number of genera with a relative abundance of less than 0.1 % and several unidentified genera were observed in D0, which were categorized as Others. The number of these genera in the group of Y19 and DYM exhibited a significant decrease, with Malikia being the predominant genus (80.6 %, 87.5 %), followed by Zoogloea (11.1 %, 3.6 %) and Rhodoferax (1.4 %, 1.3 %).

Malikia and Rhodoferax are capable of eliminating nitrates in wastewater with a low C/N ratio [47,48]. The evolutionary position of Malikia on the phylogenetic tree is closely aligned with that of hydrogen phage. This relationship is beneficial for the removal of nitrate and the degradation of COD [49–51]. Zoogloea can utilize Fe^{2+} as an electron donor for denitrification [52]. Rhodoferax is a cold-tolerant facultative bacterium capable of utilizing NO_3^--N as both an electron acceptor and a nitrogen source at low temperatures [53,54]. Considering the competitive effect of the indigenous microorganisms and no continuous additional of organic carbon source and strain Y19, the Y19 strain failed to form a dominant bacterium during operation. However, it facilitated the initiation of the nitrogen cycling process. There exists a substantial variety of semiconductor minerals in nature. When lake sediment is utilized as the source for indigenous microorganisms, the inherent semiconductor minerals present in the sediment, under light conditions, stimulate electroactive microorganisms to become the predominant bacterial population.

4. Conclusions

The photoreactive properties of heterotrophic nitrification aerobic denitrifying bacteria (HN-AD) have been experimentally confirmed. The

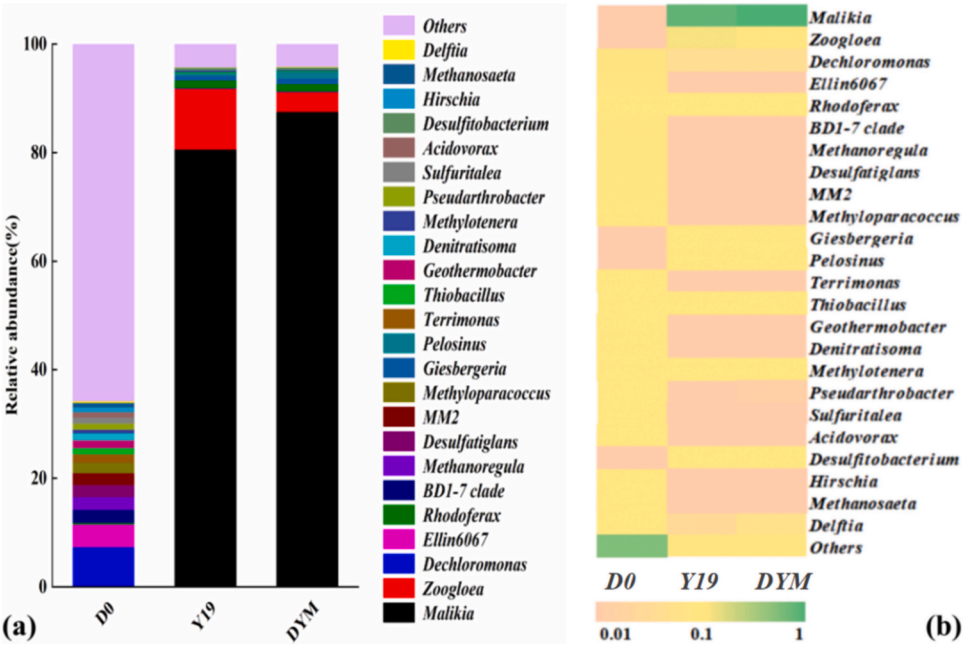

Fig. 8. Distribution of microorganisms at the genus level (a) and heat map (b).

results demonstrated that photogenerated electrons produced by magnetite can effectively stimulate and enhance the growth of strain Y19. The removal rates achieved by the coupled system of the NH_4^+-N and NO_3^--N are 4 times higher than the removal rates in the Y19 alone system. Furthermore, the photogenerated electrons generated from magnetite can enhance the metabolic activities of strain Y19 when the organic carbon source is insufficient. Notably, Fe^{2+} plays a crucial role in the reduction of NO_3^-. The denitrification mechanisms of the coupled system most likely encompass: heterotrophic nitrification and aerobic denitrification by strain Y19, photogenerated electrons reduction of magnetite, the reduction of Fe^{2+}, and the adsorption of magnetite. After 9 days of running the simulator, the magnetite-Y19 coupled system achieved removal rates of 100 % for NO_3^--N and COD, and 36 % for NH_4^+-N. This study provides innovative insights into the utilization of photogenerated electrons from semiconductor minerals by microorganisms for the treatment of wastewater with a low C/N ratio.

CRediT authorship contribution statement

Guo Liu: Writing – review & editing, Supervision, Methodology, Formal analysis. **Dian Liu:** Writing – original draft, Methodology, Investigation, Formal analysis, Conceptualization. **Mengyao Hu:** Writing – review & editing, Methodology. **Xi Ren:** Writing – review & editing, Data curation. **Yueyu Ran:** Investigation, Data curation. **Tianlie Luo:** Supervision, Methodology, Writing – review & editing. **Willie J. G.M. Peijnenburg:** Writing – review & editing.

Declaration of competing interest

The authors declare that they have no known competing financial interests or personal relationships that could have appeared to influence the work reported in this paper.

Acknowledgments

This study was financially supported by the National Key Research and Development Program of China (2023YFC3207300), the National Natural Science Foundation of China (No. 42307375), Chengdu University of Technology 2023 Young and Middle-aged Backbone Teachers Development Funding Program (No. 10912-JXGG2023-07746) and State Key Laboratory of Geohazard Prevention and Geoenvironment Protection Independent Research Project (No. SKLGP2023Z022).

Appendix A. Supplementary data

Supplementary data to this article can be found online at https://doi.org/10.1016/j.jwpe.2025.106942.

Data availability

Data will be made available on request.

References

[1] Y. Yan, H. Lu, J. Zhang, S. Zhu, Y. Wang, Y. Lei, et al., Simultaneous heterotrophic nitrification and aerobic denitrification (SND) for nitrogen removal: a review and future perspectives, Environmental Advances (2022) 9, https://doi.org/10.1016/j.envadv.2022.100254.

[2] S. Barroso-Solares, B. Merillas, P. Cimavilla-Román, M.A. Rodriguez-Perez, J. Pinto, Enhanced nitrates-polluted water remediation by polyurethane/sepiolite cellular nanocomposites, J. Clean. Prod. 254 (2020) 120038, https://doi.org/10.1016/j.jclepro.2020.120038.

[3] H. Dai, T. Han, T. Sun, H. Zhu, X. Wang, X. Lu, Nitrous oxide emission during denitrifying phosphorus removal process: a review on the mechanisms and influencing factors, J. Environ. Manage. 278 (2021) 111561, https://doi.org/10.1016/j.jenvman.2020.111561.

[4] C. Yang, Y. Chen, O. Kun, J. Yang, L. Jinping, Current research situation and prospect of ammonia nitrogen wastewater treatment technology, Industrial Water Treatment 38 (2018) 1–5, https://doi.org/10.11894/1005-829x.2018.38(3).001.

[5] J. Yang, L. Jiang, Z. Guo, E.K. Sarkodie, K. Li, J. Shi, et al., The cd immobilization mechanisms in paddy soil through ureolysis-based microbial induced carbonate precipitation: emphasis on the coexisting cations and metatranscriptome analysis, J. Hazard. Mater. 465 (2024) 133174, https://doi.org/10.1016/j.jhazmat.2023.133174.

[6] H. Dai, Y. Sun, D. Wan, H.N. Abbasi, Z. Guo, H. Geng, et al., Simultaneous denitrification and phosphorus removal: a review on the functional strains and activated sludge processes, Sci. Total Environ. 835 (2022) 155409, https://doi.org/10.1016/j.watres.2017.04.069.

[7] L.A. Robertson, J.G. Kuenen, Combined heterotrophic nitrification and aerobic denitrification in Thiosphaera pantotropha and other bacteria, Antonie Van Leeuwenhoek 57 (3) (1990) 139–152, https://doi.org/10.1007/BF00403948.

[8] H. Xi, X. Zhou, M. Arslan, Z. Luo, J. Wei, Z. Wu, et al., Heterotrophic nitrification and aerobic denitrification process: promising but a long way to go in the wastewater treatment, Sci. Total Environ. 805 (2022) 150212, https://doi.org/10.1016/j.scitotenv.2021.150212.

[9] L. Xia, X.M. Li, W.H. Fan, J.L. Wang, Heterotrophic nitrification and aerobic denitrification by a novel *Acinetobacter sp.* ND7 isolated from municipal activated sludge, Bioresour. Technol. 301 (2020) 8, https://doi.org/10.1016/j.biortech.2020.122749.

[10] H.-Y. Tang, C. Yang, T. Ueki, C.C. Pittman, D. Xu, T.L. Woodard, et al., Stainless steel corrosion via direct iron-to-microbe electron transfer by *Geobacter species*, ISME J. 15 (10) (2021) 3084–3093, https://doi.org/10.1038/s41396-021-00990-2.

[11] W. Shao, Y. Qian, X. Zhai, L. Xu, H. Guo, M. Zhang, et al., Mechanisms of nanoscale zero-valent iron mediating aerobic denitrification in *pseudomonas stutzeri* by promoting electron transfer and gene expression, Bioresour. Technol. 394 (2024) 130202, https://doi.org/10.1016/j.biortech.2023.130202.

[12] Y. Liao, S. Li, X. Zhu, Z. Dang, S. Tang, G. Ji, The promotion and inhibition effect of graphene oxide on the process of microbial denitrification at low temperature, Bioresour. Technol. 340 (2021) 125636, https://doi.org/10.1016/j.biortech.2021.125636.

[13] I. Kim, D.K. Cha, Effect of low temperature on abiotic and biotic nitrate reduction by zero-valent Iron, Sci. Total Environ. 754 (2021) 6, https://doi.org/10.1016/j.scitotenv2020.142410.

[14] S. Kato, K. Hashimoto, K. Watanabe, Iron-oxide minerals affect extracellular electron-transfer paths of *Geobacter spp*, Microbes Environ. 28 (1) (2013) 141–148, https://doi.org/10.1264/jsme2.me12161.

[15] L. Zhuang, J. Tang, Y. Wang, M. Hu, S. Zhou, Conductive iron oxide minerals accelerate syntrophic cooperation in methanogenic benzoate degradation, J. Hazard. Mater. 293 (2015) 37–45, https://doi.org/10.1016/j.jhazmat.2015.03.039.

[16] W. Ying, L. Fangbai, L. Tongxu, Advances in the semiconductor-mediated electron transfer mechanism at microbe-mineral interface, Adv. Earth Science 31 (2016) 347–356, https://doi.org/10.11867/j.issn.1001-8166.2016.04.0347.

[17] X. Gu, J. Leng, J. Zhu, K. Zhang, J. Zhao, P. Wu, et al., Influence mechanism of C/N ratio on heterotrophic nitrification- aerobic denitrification process, Bioresour. Technol. 343 (2022) 126116, https://doi.org/10.1016/j.biortech.2021.126116.

[18] S. Huang, M. Chen, Y. Diao, Q. Feng, R.J. Zeng, S. Zhou, Dissolved organic matter acting as a microbial photosensitizer drives photoelectrotrophic denitrification, Environ. Sci. Technol. 56 (7) (2022) 4632–4641, https://doi.org/10.1021/acs.est.1c07556.

[19] S. Cui, Y. Si, X.Z. Fu, H.H. Li, X.M. Wang, W.Z. Du, et al., Intracellularly-photosensitized bio-hybrid with biogenic quantum dots for enhanced wastewater denitrification, Chem. Eng. J. (2023) 457, https://doi.org/10.1016/j.cej.2022.141237.

[20] S. Pi, W. Yang, W. Feng, R. Yang, W. Chao, W. Cheng, et al., Solar-driven waste-to-chemical conversion by wastewater-derived semiconductor biohybrids, Nature Sustainability 6 (12) (2023) 1673–1684, https://doi.org/10.1038/s41893-023-01233-2.

[21] T. Tian, Semiconductor-mediated extracellular electron transport of microorganisms under light excitation, Southeast University (2020), https://doi.org/10.27014/d.cnki.gdnau.2020.001241.

[22] H.L. Dong, A.H. Lu, Mineral-microbe interactions and implications for remediation, Elements 8 (2) (2012) 95–100, https://doi.org/10.2113/gselements.8.2.95.

[23] F. Qian, H.Y. Wang, Y.C. Ling, G.M. Wang, M.P. Thelen, Y. Li, Photoenhanced electrochemical interaction between *Shewanella* and a hematite nanowire photoanode, Nano Lett. 14 (6) (2014) 3688–3693, https://doi.org/10.1021/nl501664n.

[24] G.P. Ren, Y. Sun, Y. Ding, A.H. Lu, Y. Li, C.Q. Wang, et al., Enhancing extracellular electron transfer between *Pseudomonas aeruginosa* PAO1 and light driven semiconducting birnessite, Bioelectrochemistry 123 (2018) 233–240, https://doi.org/10.1016/j.bioelechem.2018.06.003.

[25] Q. Cao, Effect of microorganisms on phenol-quinone transformation of degraded peatlands mediated by semiconductor mineral photocatalysis, Southwest University of Science and Technology (2022), https://doi.org/10.27415/d.cnki.gxngc.2022.000636.

[26] R. Ding, W.F. Yan, Y. Wu, Y. Xiao, H.Y. Gang, S.H. Wang, et al., Light-excited photoelectrons coupled with bio-photocatalysis enhanced the degradation efficiency of oxytetracycline, Water Res. 143 (2018) 589–598, https://doi.org/10.1016/j.watres.2018.06.068.

[27] D.R. Lovley, Syntrophy goes electric: direct interspecies electron transfer, Annu. Rev. Microbiol. 71 (71) (2017) 643–664, https://doi.org/10.1146/annurev-micro-030117-020420.

[28] J.M. Duan, H.D. Fang, B. Su, J.F. Chen, J.M. Lin, Characterization of a halophilic heterotrophic nitrification-aerobic denitrification bacterium and its application on

treatment of saline wastewater, Bioresour. Technol. 179 (2015) 421–428, https://doi.org/10.1016/j.biortech.2014.12.057.
[29] K. Fu, X. Cao, X.Z. Meng, Z.L. Zhu, D. Qian, Characteristics of nitrite accumulation during wastewater denitrification, Huanjing Kexue/Environmental Science 32 (2011) 1660–1664, https://doi.org/10.13227/j. hjkx.2011.06.035.
[30] T. Song, X. Zhang, J. Li, X. Wu, H. Feng, W. Dong, A review of research progress of heterotrophic nitrification and aerobic denitrification microorganisms (HNADMs), Sci. Total Environ. 801 (2021) 149319, https://doi.org/10.1016/j.scitotenv.2021.149319.
[31] W. Li, Advanced Nitrogen Bioremoval Process by Combinning Denitratation with Anammox, Zhejiang University, 2017. https://cnki.wsp2.cn/kcms2/article/abstract?v=VIrt19joK6iM5TJ1Ufpz_f5cDe3-ovBkN86oigZHKTa39Ctr2Y4gZWYXcG8tsIHAcK4Tu71H8PM-gGRwwHppxVsc1wVlbJcm5-jr9KeZtlxBOzJkLwIJ6MrxcvP6hQw_G9WSRcT0KjOH1FO2kr6BuOaGkJQuPxv1xiVs9ZIrYKjwP7fndRJhjuKpKty5mvz7ruNF9J0NpO4=&uniplatform=NZKPT&language=CHS.
[32] J. Ye, A. Hu, G. Ren, M. Chen, J. Tang, P. Zhang, et al., Enhancing sludge methanogenesis with improved redox activity of extracellular polymeric substances by hematite in red mud, Water Res. 134 (MAY1) (2018) 54–62, https://doi.org/10.1016/j.watres.2018.01.062.
[33] X. Liu, Q. Zhang, X. Yang, D. Wu, Y. Li, H. Di, Isolation and characteristics of two heterotrophic nitrifying and aerobic denitrifying bacteria, *Achromobacter sp.* strain *HNDS-1* and *Enterobacter sp.* strain HNDS-6, Environ. Res. 220 (2023) 115240, https://doi.org/10.1016/j.envres.2023.115240.
[34] Y. Liu, Y.Y. Wan, Z. Ma, W.H. Dong, X.S. Su, X.F. Shen, et al., Effects of magnetite on microbially driven nitrate reduction processes in groundwater, Sci. Total Environ. 855 (2023) 10, https://doi.org/10.1016/j.scitotenv.2022.158956.
[35] M. Sheng, Z. Ye, F. Zhu, D. Pan, S. Shao, X. Wu, New insights into nitrogen removal by divalent iron-enhanced moving bed biofilm reactor: performance, interfacial interaction and co-occurrence network, Bioresour. Technol. 399 (2024) 130621, https://doi.org/10.1016/j.biortech.2024.130621.
[36] S.T. Chen, B.H. Zhou, H.L. Chen, R.F. Yuan, Iron mediated autotrophic denitrification for low C/N ratio wastewater: a review, Environ. Res. 216 (2023) 16, https://doi.org/10.1016/j.envres.2022.114687.
[37] D.Q. Cui, T.E. Eriksen, Reduction of pertechnetate by ferrous iron in solution: influence of sorbed and precipitated Fe(II), Environ. Sci. Technol. 30 (7) (1996) 2259–2262, https://doi.org/10.1021/es9506263.
[38] X.Q. Zhou, Y.L. Wang, X. Tan, Y.Q. Sheng, Y.B. Li, Q. Zhang, et al., Genomics and nitrogen metabolic characteristics of a novel heterotrophic nitrifying-aerobic denitrifying bacterium *Acinetobacter oleivorans AHP123*, Bioresour. Technol. 375 (2023) 8, https://doi.org/10.1016/j.biortech.2023.128822.
[39] X. Xia, Y. Zhai, Y. Teng, Microbial response to biogeochemical profile in a perpendicular riverbank filtration site, Ecotoxicol. Environ. Saf. 244 (2022) 114070, https://doi.org/10.1016/J.ECOENV.2022.114070.
[40] A. Bose, E.J. Gardel, C. Vidoudez, E.A. Parra, P.R. Girguis, Electron uptake by iron-oxidizing phototrophic bacteria, Nat. Commun. 5 (2014) 7, https://doi.org/10.1038/ncomms4391.
[41] M. Waki, T. Yasuda, H. Yokoyama, D. Hanajima, A. Ogino, K. Suzuki, et al., Nitrogen removal by co-occurring methane oxidation, denitrification, aerobic ammonium oxidation, and anammox, Appl. Microbiol. Biotechnol. 84 (5) (2009) 977–985, https://doi.org/10.1007/s00253-009-2112-7.
[42] H. Lu, K. Chandran, D. Stensel, Microbial ecology of denitrification in biological wastewater treatment, Water Res. 64 (2014) 237–254, https://doi.org/10.1016/j.watres.2014.06.042.
[43] Y. Fang, F. Wang, X.B. Jia, C.Q. Lin, H. Zhang, L.J. Chen, et al., Effect of green manure and reduced chemical fertilizer load on the community of soil nitrogen-fixing bacteria, Journal of Agro-Environment Science 37 (2018) 1933–1941, https://doi.org/10.11654/jaes.2018-0509.
[44] S. Chen, Z. Liao, Y. Hu, Effects of nitrogen removal in black and odorous water using Iron-carbon interior electrolysis combined with *ipomoea Aquatica*, Journal of South China Normal University (Natural Science Edition) 51 (5) (2019) 38–48, https://doi.org/10.6054/j.jscnun.2019083.
[45] J.M. Sun, X.D. Liu, Y.Q. Tang, M. Li, Y.N. Zou, Microorganism and biostimulant collaboratively remediate river sediment-influence of biostimulant quantity on repair performance, Zhongguo Huanjing Kexue/China Environmental Science 39 (2019) 351–357, https://doi.org/10.19674/j.cnki.issn1000-6923.2019.0043.
[46] L. Ye, M.-F. Shao, T. Zhang, A.H.Y. Tong, S. Lok, Analysis of the bacterial community in a laboratory-scale nitrification reactor and a wastewater treatment plant by 454-pyrosequencing, Water Res. 45 (15) (2011) 4390–4398, https://doi.org/10.1016/j.watres.2011.05.028.
[47] P. Zhang, Y. Peng, J. Lu, J. Li, H. Chen, L. Xiao, Microbial communities and functional genes of nitrogen cycling in an electrolysis augmented constructed wetland treating wastewater treatment plant effluent, Chemosphere 211 (2018) 25–33, https://doi.org/10.1016/j.chemosphere.2018.07.067.
[48] B. Braun, J. Schröder, H. Knecht, U. Szewzyk, Unraveling the microbial community of a cold groundwater catchment system, Water Res. 107 (2016) 113–126, https://doi.org/10.1016/j.watres.2016.10.040.
[49] W. Li, C.W. Xiao, Y. Zhao, Q.Q. Zhao, R. Fan, J.J. Xue, Electrochemical reduction of high-concentrated nitrate using Ti/TiO2 nanotube Array anode and Fe cathode in dual-chamber cell, Catal. Lett. 146 (12) (2016) 2585–2595, https://doi.org/10.1007/s10562-016-1894-3.
[50] L.H. Su, K. Li, H.B. Zhang, M.H. Fan, D.W. Ying, T.H. Sun, et al., Electrochemical nitrate reduction by using a novel Co_3O_4/Ti cathode, Water Res. 120 (2017) 1–11, https://doi.org/10.1016/j.watres.2017.04.069.
[51] J.L. Duan, J.W. Sun, M.M. Ji, Y. Ma, Z.T. Cui, R.K. Tian, et al., Indicatory bacteria and chemical composition related to sulfur distribution in the river-lake systems, Microbiol. Res. 236 (2020) 9, https://doi.org/10.1016/j.micres.2020.126453.
[52] Y.Z. Yang, A. Ali, J.F. Su, L. Xu, X.M. Wang, E.L. Liang, Simultaneous removal of nitrate, tetracycline, and Pb(II) by iron oxidizing strain *Zoogloea sp.* FY6: performance and mechanism, Bioresour. Technol. 360 (2022) 10, https://doi.org/10.1016/j.biortech.2022.127569.
[53] S. Yao, J.R. Ni, Q. Chen, A.G.L. Borthwick, Enrichment and characterization of a bacteria consortium capable of heterotrophic nitrification and aerobic denitrification at low temperature, Bioresour. Technol. 127 (2013) 151–157, https://doi.org/10.1016/j.biortech.2012.09.098.
[54] K. Kosek, A. Luczkiewicz, K. Kozioł, K. Jankowska, M. Ruman, Ż. Polkowska, Environmental characteristics of a tundra river system in Svalbard. Part 1: bacterial abundance, community structure and nutrient levels, Sci. Total Environ. 653 (2019) 1571–1584, https://doi.org/10.1016/j.scitotenv.2018.11.378.